https://doi.org/10.5194/egusphere-2026-2652
Preprint. Discussion started: 10 June 2026

EarthCARE MSI Level-1 Data: First In-Orbit Calibration and Validation

Sebastian Bley[1], Anja Hünerbein[1], Edward Baudrez[5], Nils Madenach[1], Nicole Docter[1], René Preusker[2], Michael Eisinger[3], Fabien Marnas[4], Antje Ludewig[6], Manuel Ángel Ruiz Saldaña[7], Cameron Bean[7], Shweta Agarwal[7], Lennart Zimmermann[8], and Timon Hummel[9]

[1]Leibniz Institute for Tropospheric Research, Leipzig, Germany
[2]Freie Universität Berlin (FUB), Berlin, Germany
[3]European Space Agency (ESA), ECSAT, Harwell, United Kingdom
[4]European Space Agency (ESA), ESTEC, Noordwijk, The Netherlands
[5]Royal Meteorological Institute of Belgium, Brussels, Belgium
[6]Royal Netherlands Meteorological Institute (KNMI), De Bilt, the Netherlands
[7]GMV, Airspeed 2, Eighth Street, Harwell Science and Innovation Campus, Didcot, Oxfordshire, OX11 0RL, United Kingdom
[8]Airbus Defence and Space GmbH, Germany
[9]European Space Agency (ESA), ESRIN, Frascati, Italy

Correspondence: Sebastian Bley, bley@tropos.de

Abstract. The successful launch of the EarthCARE satellite on 28 May 2024, with its unique combination of active and passive instruments, enables new insights into advanced cloud-aerosol-radiation interactions in the atmosphere. The Multi-Spectral Imager (MSI) onboard the EarthCARE satellite provides horizontal observations of reflected visible, near-infrared, and short-wave infrared (VNS) radiation and emitted thermal infrared (TIR) radiation across a 150-km swath. Following 1.5 years of calibration and validation, the MSI instrument is performing very well.

This paper focuses on the main findings of the validation and calibration of the MSI Level-1 data since the launch. One major improvement in the MSI Level-1 processing was the introduction of band-specific pixel geolocation and inter-band coregistration corrections. These improvements have been shown to achieve the necessary instrument performance, successfully meeting the specifications for geolocation accuracy of $\pm$500 meters and coregistration accuracy of $\pm$0.3 pixels.

The radiometric accuracy of MSI was assessed against the Flexible Combined Imager (FCI) onboard the Meteosat Third Generation (MTG) satellite using collocated cloud scenes. The results showed systematic offsets in MSI Level-1 VNS radiances compared to the corresponding FCI spectral bands. These findings led to the conclusion to perform an ad-hoc vicarious calibration of the MSI VNS radiances against FCI. The initial verification results for the improved and reprocessed MSI Level-1 *BA* dataset confirm the successful mitigation of the observed offsets between MSI and FCI with relative biases below 1%.

In addition, the VNS reflectances exhibited unexplained across-track variations that could not be attributed to the radiance measurements. Monitoring of the spectral solar irradiance, measured by MSI's onboard diffusers, revealed across-track artifacts and day-to-day variations exceeding expected solar variability. Therefore, the measured spectral solar irradiance has been replaced by theoretical values in the MSI Level-1 product. All of these updates led to a significantly improved radiometric and geometric stability.

https://doi.org/10.5194/egusphere-2026-2652
Preprint. Discussion started: 10 June 2026

1 Introduction

The Multi-Spectral Imager is one of the four instruments onboard the ESA-JAXA EarthCARE satellite, providing horizontal information of the reflected visible, near-infrared, and shortwave infrared (VNS) radiation, as well as thermal infrared (TIR) radiation emitted by aerosols, clouds and the Earth surface. These measurements extend the vertical profiles of Atmospheric Lidar (ATLID) and the Cloud Profiling Radar (CPR) into three-dimensional scenes. This capability supports radiative closure studies, which compare modeled radiation fluxes using input from ATLID, CPR and MSI with measurements from the Broadband Radiometer (BBR).

MSI is a nadir-pointing push-broom imager with a 150 km swath width and 500 m pixel resolution (Wehr et al., 2023). To minimize the number of pixels affected by sunglint, the swath is offset, 115 km to the left and 35 km to the right of nadir. MSI features seven spectral channels, including four bands in the visible, near-infrared and short-wave infrared regions (VIS: 0.67 μm; NIR: 0.865 μm; SWIR-1: 1.65 μm; SWIR-2: 2.21 μm) and three in the thermal infrared (TIR-1: 8.8 μm; TIR-2: 10.8 μm; TIR-3: 12.0 μm). The VIS, NIR and SWIR-2 bands have a spectral response function with a width of 0.02 μm, while the SWIR-1 band has a broader band width of 0.05 μm. While other passive satellite imagers such as MODIS, VIIRS, AVHRR, ABI, SEVIRI and FCI offer more spectral bands, only MSI provides radiance and brightness temperature measurements accurately co-located with the footprint of the active instruments with consistent viewing geometry. This configuration not only supplies the horizontal scene context to the profile measurements made by ATLID and CPR, but also connects aerosol and cloud microphysics with broadband radiation as measured by BBR.

Following the EarthCARE launch, a six-month commissioning phase started, in which a series of activities were performed, including data acquisition verification, instrument health monitoring, and performance assessment to ensure smooth operation of all four instruments. MSI was turned on 11 June 2024, followed by a decontamination phase of one-month. After a successful transition to measurement mode, the first acquisition of MSI Level-1 data was on 16 July 2024. By the end of 2024, ESA had successfully completed the EarthCARE commissioning phase, confirming nominal operations of all four instruments and the readiness of all processors.

Among all activities performed in the first year of operation, this paper focuses on the evaluation and improvement of the geometric and radiometric performance of the MSI Level-1 radiances and brightness temperatures. The geometric performance is evaluated in terms of geolocation accuracy and inter-channel coregistration. These aspects are critical for the consistent interpretation of multi-spectral observations and for downstream retrieval products. For multi-sensor comparison and for long-term trend studies, accurate pixel registration is even more important (Le Moigne et al., 2011). Since the EarthCARE mission provides synergistic multi-instrument products, correcting the MSI pixel geolocation and coregistration was the primary focus during the begin of the commissioning phase.

Radiometric noise, accuracy, uncertainty, and their long-term changes are important characteristics that must to be evaluated throughout the whole mission (Cao et al., 2013). This is typically done using on-board calibration systems, such as internal black-body targets for the calibration of the TIR bands and sun diffusers for measuring the solar spectral irradiance (Cao et al., 2014). However, absolute radiometric accuracy requires validation against independent reference measurements. Xiong et al.

https://doi.org/10.5194/egusphere-2026-2652
Preprint. Discussion started: 10 June 2026

(2019) showed that, for MODIS, on-board calibration systems provide continuous monitoring of the instrument performance (e.g., through on-board diffusers), whereas validation and refinement of the absolute radiometric calibration requires vicarious calibration.

We used collocated observations from the Flexible Combined Imager (FCI) aboard Meteosat Third Generation, from airborne imagers and ground-based remote sensing sites for the validation of the radiometric performance. These comparisons showed systematic biases in MSI Level-1 VNS radiances and across-track artifacts in the reflectance. Following these observed issues, we performed an ad-hoc vicarious calibration using FCI which is presented in this article.

Vicarious calibration over pseudo invariant calibration sites (PICS) is a widely used method for the in-flight radiometric calibration of passive satellite imagers and has been applied for more than 25 years (Helder et al., 2013). PICS are well suited for long-term monitoring of the radiometric performance due to their high temporal stability with almost no seasonal variability in surface reflectance (Khadka et al., 2021).

VIIRS used vicarious calibration sites over desert and the Antarctica (Dome C site) in addition to the on-board calibration system for routine monitoring of the radiometric performance (Cao et al., 2013). They showed that VIIRS agrees well with MODIS within 2 % for these vicarious calibration sites.

ESA developed a tool for radiometric intercomparison of passive satellite sensors over terrestrial targets (European Space Agency, 2016). It is based on a radiative transfer model to simulate top-of-atmosphere (TOA) observations of the visible and near-infrared range over PICS (e.g., Libya-4 site), calibrated on four years of MERIS data (Bouvet, 2014).

de Vries et al. (2007) described an operational vicarious calibration procedure for Landsat, based on cross-satellite calibration between different Landsat sensors. This approach demonstrated improved performance compared to the on-board calibration system and effectively removed artificial trends in long-term vegetation observations over Australia. EUMETSAT developed a Deep Convective Cloud (DCC) reference model for vicarious calibration of the SEVIRI instrument on Meteosat, achieving calibration coefficient uncertainties of approximately ± 1.5 % in the VIS bands and ± 3 % in the NIR bands, which is comparable to the standard pseudo-invariant desert and ocean targets (Rayference, 2017). FCI relies on an in-orbit inter-satellite calibration approach as it has lost its on-board calibration system. To mitigate this challenge, Mousivand et al. (2025) used the Infrared Atmospheric Sounding Interferometer (IASI) hyperspectral instrument aboard the Metop-B and Metop-C satellites for calibration of the FCI IR bands and the Mission Integrated Calibration Monitoring Inter-Calibration System (MICMICS) for calibration of the VNS bands.

Reliable vicarious calibration over PICS requires large cloud free data samples. This is particularly challenging for satellite images with a narrow swath, such as MSI. Combined with its long repeat cycle of 25 days, it is a time consuming process for MSI to acquire a sufficient data sample.

Taking these limitations into account, we decided during the first year of MSI in operation to use deep convective cloud targets measured simultaneously with FCI and MSI under similar viewing geometries to perform an ad-hoc vicarious calibration. Stable Level-1 reflectances are an important prerequisite for improving the MSI Level-2A cloud and aerosol products, including the Cloud Mask (MSI_CM__2A; Hünerbein et al. (2023)), Cloud Optical and Physical Properties (MSI_COP_2A; Hünerbein et al. (2024)) and the Aerosol Optical Thickness products (MSI_AOT_2A; Docter et al. (2023)) on the European

https://doi.org/10.5194/egusphere-2026-2652
Preprint. Discussion started: 10 June 2026

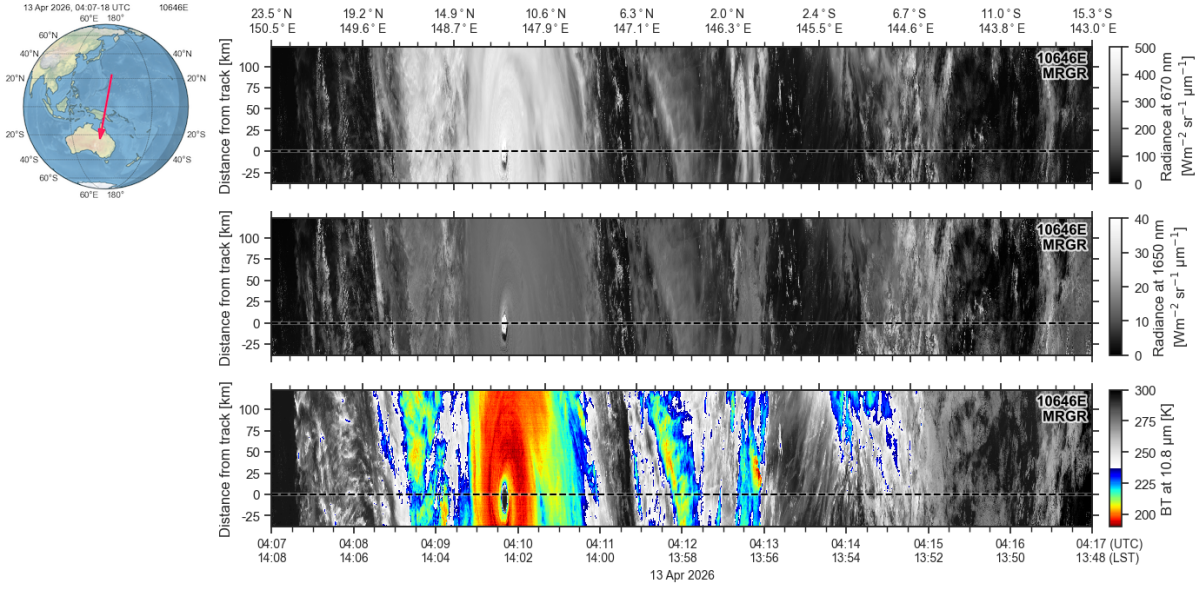

Figure 1. VIS (0.67 μm) and NIR (1.65 μm) radiance and color-enhanced TIR-2 (10.8 μm) brightness temperature of EarthCARE frame 10646E, capturing Super Typhoon Sinlaku on 13 April 2026 over the Northwest Pacific. The red arrow in the map figure shows the descending EarthCARE track.

side as well as the Cloud Products (MSI_CLP_2A; Japan Aerospace Exploration Agency (2024)) on the Japanese side. Some of these Level-2a MSI-only products are subsequently used in synergistic Level-2b algorithms alongside data from the Atmospheric Lidar (ATLID), Cloud Profiling Radar (CPR), and Broad-Band Radiometer (BBR). Consequently, uncertainties in the MSI Level-2a products propagate into these multi-instrument retrievals.

ESA has currently announced an extension of EarthCARE mission targets from the initial 3-year lifetime to a 10-year and beyond mission (European Space Agency, 2025). The MSI instrument is expected to measure throughout the entire mission, confirming the need for long-term validation and calibration of the radiometric accuracy.

Section 2 provides an overview of the MSI Level-1 products, including the processor baseline evolution. Section 3 presents the geolocation and coregistration assessment. Section 4) describes the radiometric calibration of the VNS bands, including the ad-hoc vicarious calibration, while section 5 addresses the radiometric calibration of the TIR bands. Section 6 summarizes the results and global statistics from the first one and a half years of MSI Level-1 data, while Section 6.2 provides the first statistical verification against FCI. Conclusions are given in Section 7.

2 MSI Level-1 data products

The MSI level 1 processor uses the raw instrument level 0 data, including the digital counts and the full ancillary information, to produce the nominal level 1b data (called M-NOM) with radiometrically calibrated spectral radiances in $Wm^{-2}\mu m^{-1}sr^{-1}$ for

https://doi.org/10.5194/egusphere-2026-2652
Preprint. Discussion started: 10 June 2026

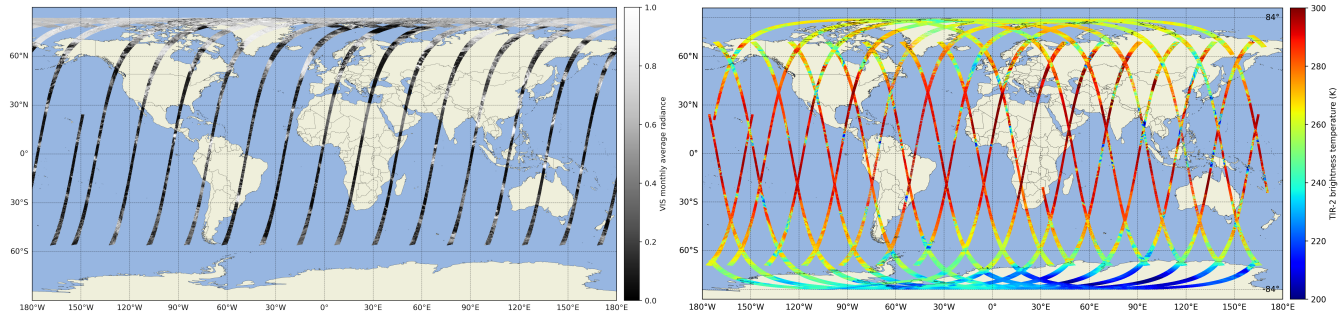

Figure 2. 24-hour MSI VIS reflectance (left) and TIR-2 brightness temperature in K (right) on 2 June 2025.

the Visible, Near infrared and Short wave infrared (VNS) bands and with brightness temperatures in K for the Thermal InfraRed (TIR) bands (Eisinger et al., 2024). MSI level 1b data is geolocated on a native grid individually for each band. To make it ready to use for the level 2 data processors, level 1b data is processed into level 1c data (called M-RGR) with co-registration applied to match all bands to a common grid. Each MSI M-RGR dataset contains 384 across-track and approximately 11900 along-track pixels for each of the seven spectral bands. Around 360 of the 384 across-track pixel are illuminated by the reflected sun light and the remaining "wing-pixels" are used for monitoring dark-current offsets. All MSI Level-1 data products since 16 July 2024 are available to users through the ESA Multi-Mission Algorithm and Analysis Platform (MAAP: https://portal.maap.eo.esa.int/earthcare/).

One complete orbit is divided into eight frames, each defined by fixed latitudinal boundaries and identified by a frame ID (*A*–*H*).Frame *C* is centered over the Arctic and frame *G* over the Antarctic. Frames *E* and *A* correspond to the Tropics during daytime and nighttime, respectively. Frames *D* and *F* cover the Northern and Southern mid-latitudes, while frames *B* and *H* serve as their nighttime counterparts. The detailed definition of these frames can be found in the CPR Level-1 Product Definition Document (Team).

Figure 2 shows 24-hours of MSI observations of the VIS reflectance and the TIR-2 brightness temperature (K) on 2 June 2025. It illustrates the daily coverage achieved with the 150 km swath, which is narrower than the wide-swath imagers such as MODIS (~2330 km), Sentinel-3 OLCI (~1270 km) or VIIRS (~3000 km). However, this focused swath ensures high spatial resolution (500 m) and accurate co-registration with EarthCARE's ATLID and CPR footprint. Figure 2 shows a summer day in the northern hemisphere, with minimum brightness temperatures below 200 K over Antarctica and the tops of tropical deep convective clouds, and maximum temperatures over cloud-free land in the northern mid-latitudes. On the other side, it shows how bright or dark the Earth appears on that day at the TOA seen from the MSI VIS band. MSI has a global coverage of roughly 84° North to 84° South. For the reflectance composite, data with solar zenith angle > 80° is rejected.

2.1 MSI Level-1 data evolution

During the first one and a half years of MSI in operation, several corrections and improvements have led to multiple Level-1 processor baseline updates. The processor version labeling uses two characters: the first character indicates the reprocessing

https://doi.org/10.5194/egusphere-2026-2652
Preprint. Discussion started: 10 June 2026

Level-1 processor baseline	Start date	End date	Main updates
AA	16.07.2024	20.09.2024	Pre-operational processor version.
AD	20.09.2024	13.01.2025	Update of TIR channel across-track resolved calibration maintenance gains.
AE	13.01.2025	27.01.2025	Update of pixel geolocation.
AF	27.01.2025	27.05.2025	Update of VNS bi-directional scattering distribution function (BSDF) and band-to-band co-registration
BA	16.07.2024	18.11.2025	Update of VNS maintenance gains via ad-hoc vicarious calibration and use of theoretical TSIS-2-based solar spectral irradiance
BC	18.11.2025	present	Same processor settings and calibration as BA

Table 1. MSI Level-1 processor versions indicated by baseline names, including processing periods and main updates.

cycle, the second shows the processor version within that cycle. The baselines are in alphabetical order (ESA EarthCARE Team, 2025). When a new reprocessing cycle starts (e.g., within baseline BA), the second character starts with A again. This naming scheme provides users with the best possible data quality in quasi-near-real-time (NRT), while having regular reprocessing campaigns for improved dataset homogeneity. A Level-1 data disclaimer document is published along with each baseline version describing the main updates and limitations (ESA EarthCARE Mission Team, 2025).

Table 1 provides an overview of MSI Level-1 processor versions until now. The initial pre-operational Level-1 data carried the suffix *AA* and was available only to commissioning teams. On 13 January 2025, Level-1 data products have reached preliminary maturity status through baseline *AE* leading to public data release of Level-1 products on 14 January 2025.

Since 27 May 2025 (Operational activation of baseline *BA*), the MSI Level-1 processor includes all major improvements from the first year of in-orbit validation and calibration. This includes a correction of the pixel geolocation and coregistration, replacement of the solar irradiances measurements by theoretical values, update of the TIR calibration maintenance gains, as well as ad-hoc vicarious calibration of the VNS radiances. In summer 2025, all Level-1 data dating back to 16 July 2024 were reprocessed with this baseline version, now providing a homogeneous dataset covering almost two years. In the frame of another baseline update of Level-1 processors of other EarthCARE instruments, baseline *BC* was introduced on 18 November 2025, however with no changes corresponding to the MSI Level-1 processor.

3 Geolocation and coregistration assessment

The geometric accuracy of MSI is assessed using a feature- or intensity-based image registration approach (Le Moigne et al., 2011). The method estimates optimal along- and across-track translations between MSI observations and a reference dataset by maximizing spatial alignment over selected sub-scenes.

While more complex transformation models, including rotation or non-rigid deformation, could be applied, we have adopted a two-dimensional translation model to only correct for along- and across-track directions.

https://doi.org/10.5194/egusphere-2026-2652
Preprint. Discussion started: 10 June 2026

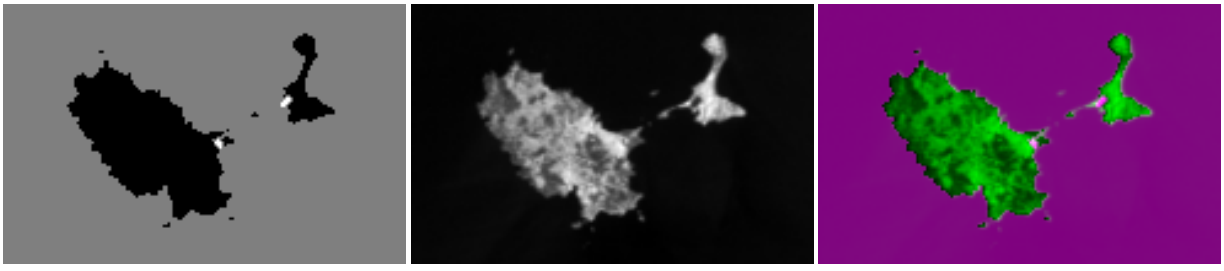

Figure 3. Example of the image registration approach for geolocation assessment over Ibiza and Formentera in the Mediterranean Sea (frame 1130D, M-NOM Level-1b). All images are geolocated on a common 500 m oblique Mercator grid. Left: Reference Copernicus Water Body Mask with colors corresponding to ocean (gray), land (black) and lakes (white). Middle: MSI VIS radiance (baseline AA) with high values shown in bright and low values in dark colors. Right: Registration diagnostic prior to optimization, highlighting coastline misalignment.

According to the EarthCARE mission requirements the geolocation accuracy of ≤ 500 m and channel coregistration of ≤ 0.30 pixels are targeted.

The Copernicus Water Body Mask (Airbus Defence and Space GmbH., 2022) is used as reference due to its high spatial accuracy ($\sim$6 m) and resolution ($\sim$30 m). Both reference and MSI data are reprojected onto a common oblique Mercator grid aligned with the satellite track at approximately 500 m resolution.

The method is applied to multiple globally distributed high-contrast scenes, primarily at land–water boundaries under clear-sky conditions to perform a statistical analysis.

3.1 Geolocation assessment

Geolocation assessment is carried out at Level 1b (M-NOM) for every MSI channel, following the approach described in section 3. To illustrate the method, the images used in the registration for one particular scene are reproduced in Figure 3. This particular channel (VIS), taken from baseline AA, happens to exhibit a small misalignment in the along-track direction, visible in the registration diagnostic image on the right.

An example demonstrating how the registration method is able to align strong gradients in the measured radiances with the land/water demarcations from the Copernicus Water Body Mask product, is shown in Figure 4. The left image displays the TIR1 channel data from frame 02011A, while the right image shows the geolocation after applying shifts from the optimization algorithm. The alignment with coastlines and lake and river edges has significantly improved. The along-track shift is estimated by the optimization to be -560 m, corresponding to a backward shift (when looking in the direction of flight). The across-track shift is estimated by the optimization to be 1008 m to the right (when looking in the direction of flight).

Performing the image registration for every channel and for every of the approximately 900 scenes distributed globally, it is possible to do a statistical analysis. The distribution of the scenes is shown in Figure A1. The majority of scenes are located at the boundary of land and large water bodies (seas and oceans), but some scenes are located at larger inland lakes or wide river deltas. In every case, the scene represented an area of high contrast in the visible or thermal radiances.

https://doi.org/10.5194/egusphere-2026-2652
Preprint. Discussion started: 10 June 2026

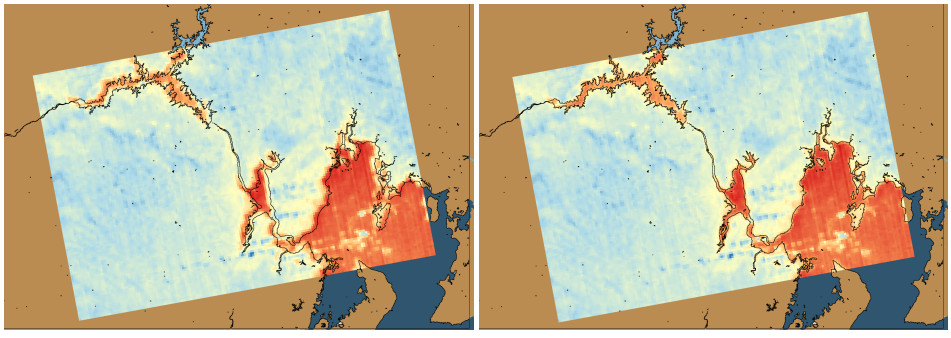

Figure 4. Example scene for the geolocation correction for frame 2011A (baseline AD), channel TIR-1 overlaid with Copernicus Water Body Mask. The left image shows the Level-1b product with original geolocation, the right image shows the result after coregistration correction. The estimated shifts are -560 m in along-track and 1008 m in across-track direction.

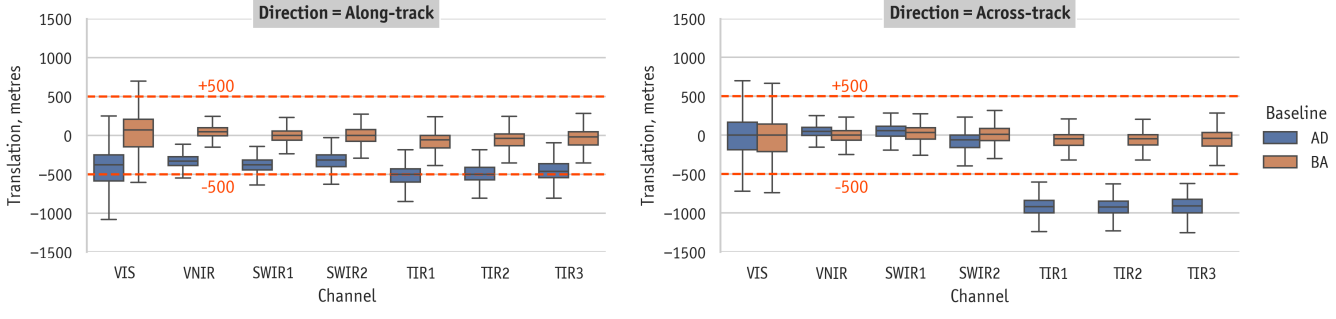

Figure 5. Statistical summary of the optimal along-track and across-track shifts obtained from the registration algorithm. All shifts are expressed in metres. The boxes represent the first, second (mean) and third quartiles, whiskers indicate 1.5 times the interquartile range (99.3% for a normal distribution). The instrument specification (+/- 500m) is shown as red, dashed lines. Positive along-track values imply shifts in flight direction, negative shifts backwards. Positive and negative across-track values indicate leftward and rightward shifts in flight direction, respectively.

https://doi.org/10.5194/egusphere-2026-2652
Preprint. Discussion started: 10 June 2026

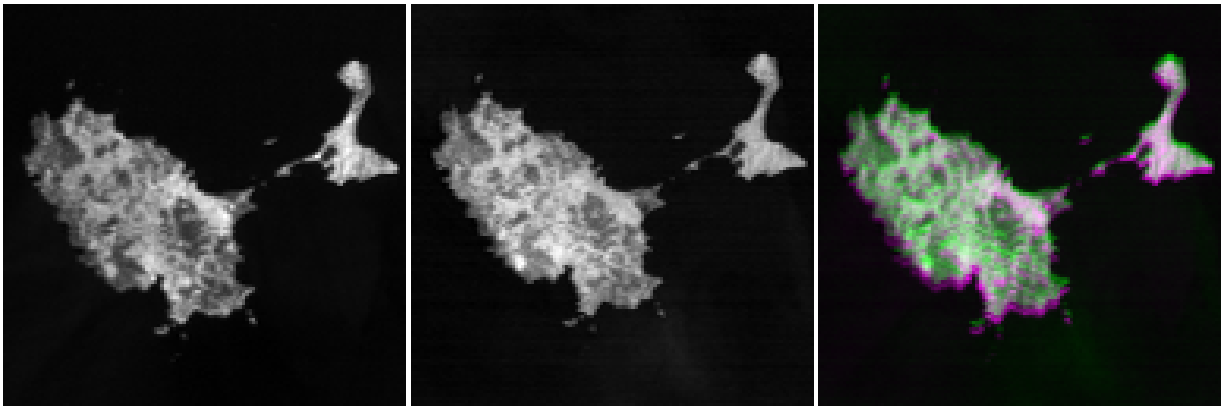

Figure 6. Example for the coregistration performance assessment for the same scene as in Fig. 3 (Ibiza and Formentera, frame 1130D, M-RGR Level-1c). Left: MSI VIS reference image (baseline AA). Middle: MSI TIR-1 image. Right: Registration diagnostic before optimization, showing the across-track misalignment between the two bands as magenta and green shadows.

The results of the statistical analysis of the registration results on the aforementioned scenes is shown in Figure 5, both for baseline AD and baseline BA. Baseline AD represents the initial geolocation performance, because no updates had been applied to the instrument pointing information at that point. It is clear that several channels are out of specification. In particular, all channels appear to be 'ahead' of where they are expected to be, which is visible as a negative along-track shift obtained from the registration algorithm. Similarly, the TIR bands appear to suffer from a significant geolocation error of almost 1 km. These findings led to an update of the pointing information in the CCDB incorporated in baseline *BA* showing a significantly improved geolocation accuracy, well within specifications for most channels. The larger uncertainty on the VIS channel is likely due to the method: the contrast between water and land surfaces is somewhat lower in the VIS channel than in the other channels, and the potential for erroneous registrations is higher. This could be addressed by performing more registrations and stricter quality control on the scenes (e.g., check for residual cloud contamination and sufficient contrast).

Up to now, suitable clear-sky scenes with land/water demarcations have been selected by hand, but an automated approach would be preferable.

3.2 Coregistration assessment

In contrast to geolocation assessment, which is performed on Level-1b (M-NOM) data, coregistration assessment is carried out using Level-1c (M-RGR) data. For each MSI channel combination, one band is registered to another band, treated as the reference image in that case, using the same approach as described in section 3.1. While geolocation assessment relies on an external reference dataset, coregistration evaluates the relative alignment between MSI channels.

https://doi.org/10.5194/egusphere-2026-2652
Preprint. Discussion started: 10 June 2026

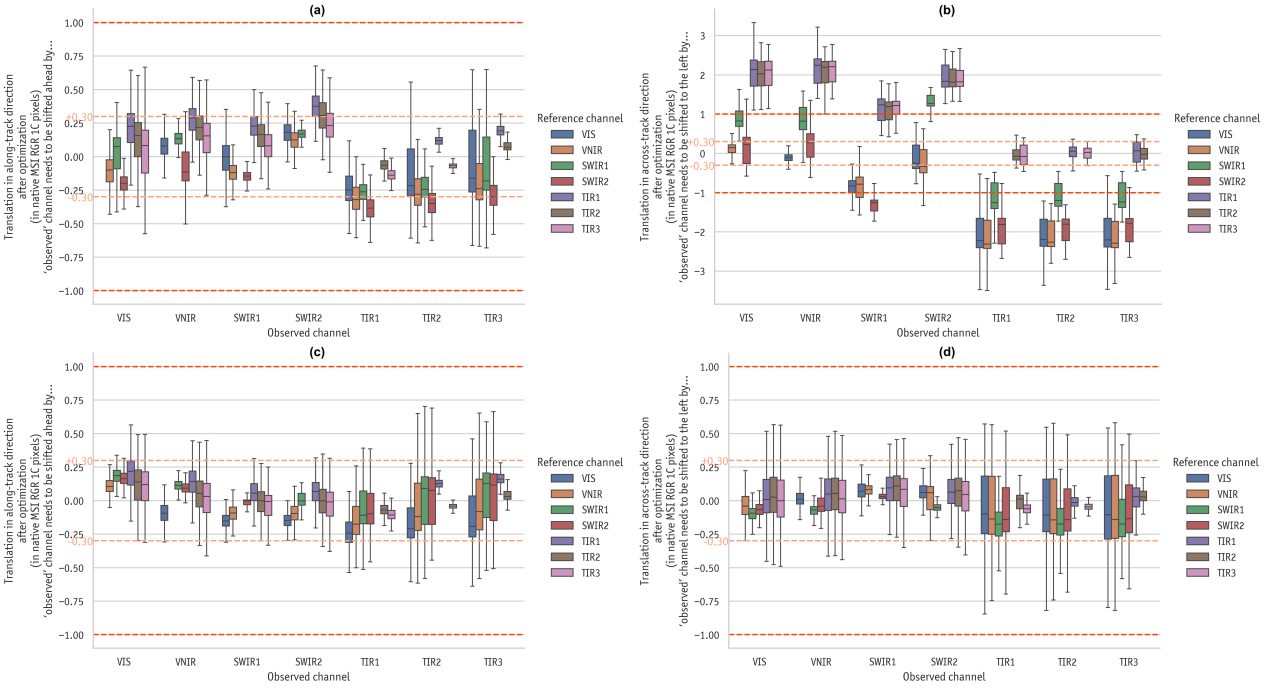

Figure 7. Statistical summary of optimal along- and across-track shifts from the registration algorithm. Panels (a) and (b) represent baseline AD, while (c) and (d) correspond to baseline BA. Translations are in fractions of an MSI pixel. Boxes show quartiles, with whiskers at 1.5 times the interquartile range. The instrument specification of ±0.3 pixels is marked by an orange dashed line. Positive shifts indicate displacements in the flight direction (along-track) and to the left (across-track), while negative values represent shifts in the opposite directions. Note that the across-track panels have a different scale.

Figure 6 illustrates the coregistration assessment for the same scene as in Figure 3 for a particular band combination of the VIS (left) and TIR-1 (middle) channel. The registration diagnostic image (Figure 6 (right)) clearly shows an across-track misalignment of nearly two pixels in baseline AA.

The same scenes as used in section 3.1 and shown in Figure A1 were also used for the coregistration assessment. The results of the statistics analysis are shown in Figure 7.

When interpreting the results in Figure 7, it should be noted that any residual geolocation error of a channel will affect the coregistration results of that channel with other channels. In other words, the geolocation errors determined in section 3.1 will be compounded into the coregistration errors shown in this section. For baseline AD (top panel of Figure 7), the along-track coregistration was generally already within specifications, while across-track coregistration was out of specification for the TIR channels because their geolocation was inaccurate. One result that does not follow from a geolocation error, is that the SWIR1 channel is showing a significant coregistration error in the across-track direction, with respect to the other VNS channels. Following these findings, an update of the instrument pointing information was implemented in baseline *BA*, resulting in significantly improved coregistration (Figure 7 bottom).

https://doi.org/10.5194/egusphere-2026-2652
Preprint. Discussion started: 10 June 2026

When evaluating the graphical results, it might appear as if the spread on the results is unacceptably large. Several factors are contributing to the spread, some of which are consequences of the evaluation method, rather than instrument performance.

Certain combinations (in particular, combinations between VNS and TIR) are more susceptible to residual cloud contamination of the scenes, which results in higher probability of erroneous registrations. This could be mitigated with stricter quality control of the selected clear-sky scenes.

The spatial interpolation of the channels to the grid of the reference channel (TIR-2), going from Level 1b to Level 1c, is performed using the nearest-neighbor method, limiting the maximum geometric accuracy that can be achieved.

There are less combinations involving VNS channels than there are combinations involving only TIR channels, since the VNS channels are only usable during daytime. In the present study, daytime scenes contribute about half the total number of scenes.

Other potential factors contributing to the spread, such as variations during an orbit, have not been investigated here.

4 VNS radiometric calibration

The MSI VNS instrument is designed to achieve a minimum of 10% absolute radiometric accuracy (Wehr, 2006; Tabak et al., 2013). For reliable aerosol and cloud retrievals, however, the goal is an absolute radiometric accuracy of 2 %, while 5 % is considered the threshold breakpoint beyond which scientific usability is significantly compromised. To reach this accuracy, gain factors for each channel must be very well characterized and regularly calibrated in-orbit.

To meet this radiometric accuracy requirement, MSI is equipped with an on-board calibration unit based on solar diffusers and dark signal measurements. It consists of a carousel with two openings (nadir and sun pointing), which allows switching between Earth observation, dark signal acquisition (both ports closed), and solar calibration (Wehr et al., 2023). The dark signal measurements are used for offset correction. Solar calibration is done by illuminating two pairs of diffusers with direct sunlight, one for VNS-NIR-SWIR-1 and one for the SWIR-2 band (Wehr et al., 2023). The first element of each pair, called Sun Diffuser 1 (SD1), is used for daily solar measurements. The second element, Sun Diffuser 2 (SD2), performs the same function but is operated only once a month to monitor the aging of SD1, which may result from contamination and exposure to solar UV associated with its more frequent use (Lobb et al., 2017).

In contrast to MODIS, where calibration gain factors are applied in reflectance space (Xiong et al., 2019), the calibration of MSI VNS bands is performed in radiance space, converting digital counts into calibrated spectral radiances ($Wm^{-2}\mu m^{-1}sr^{-1}$). This is achieved by multiplication of calibration factors to each across-track pixel. These factors include geometric factors, a band-specific digital gain, an across-track scaling factor, and a set of degradation factors, accounting for potential changes in VNS sensitivity due to variations in optical transmission or detector response (Wehr et al., 2023; de Goeij et al., 2019; Tabak et al., 2013; Albinana et al., 2011). The resulting calibrated radiances are provided in the M-RGR Level-1 product for each VNS band. The full set of calibration parameters is provided by the Calibration and Characterization Database (CCDB), including the on-ground characterization of the Bi-directional Scattering Distribution Function (BSDF) of the sun and the Earth view.

https://doi.org/10.5194/egusphere-2026-2652
Preprint. Discussion started: 10 June 2026

The MSI level-2 cloud and aerosol processors require top-of-atmosphere (TOA) spectral reflectances ρ_{TOA} as input, which rely on accurate measurements of the solar spectral irradiance. The solar spectral irradiance E_{sun} is radiometrically calibrated on-board, consistent with radiance calibration, and provided in the M-RGR Level-1 product for conversion to reflectance through the Level-2 processor using Equation 1.

$$\rho_{\text{TOA}} = \frac{\pi \cdot L_{\text{calibrated}}}{E_{sun} \cdot \cos(\theta_s)} \tag{1}$$

where:

ρ_{TOA} = Top-Of-Atmosphere reflectance (unitless)

$L_{\text{calibrated}}$ = spectral radiance ($\text{W}\cdot\text{m}^{-2}\cdot\text{sr}^{-1}\cdot\mu\text{m}^{-1}$)

E_{sun} = mean solar spectral irradiance ($\text{W}\cdot\text{m}^{-2}\cdot\mu\text{m}^{-1}$)

θ_s = solar zenith angle

While pre-launch characterization ensured accurate knowledge of spectral response and diffuser properties, in-orbit calibration mainly aims to monitor instrument degradation and update gain factors accordingly (Zimmermann et al., 2023). However during the commissioning phase, significant across-track artifacts were observed in TOA reflectances that were not present in the corresponding radiances (see Figure 8). These artifacts were traced back to the measured solar spectral irradiance, which exhibited unexpected across-track jumps and day-to-day variations exceeding those expected from theoretical solar variability. Since these artifacts are already present in Level-0 data, we assume that they are not artificially introduced by the Level-1 processor. Investigations and special measurements with the diffusers are currently underway.

These findings demonstrate that we need independent calibration and validation methods, such as vicarious calibration, to assess the absolute radiometric accuracy. The EarthCARE Mission Requirements Document (MRD) already points out the need to apply vicarious calibration to further improve the MSI VNS radiometric accuracy (Wehr, 2006).

4.1 Theoretical solar spectral irradiances

Figure 8 shows the across-track resolved daily mean VIS channel radiance (top) and reflectance (bottom), normalized by the across-track daily mean, from October 2024 until March 2026. We have generated these monitoring statistics early in the mission to identify temporal and across-track artifacts while minimizing the influence of surface and atmospheric variability. While the across-track behavior of the radiance is temporally stable over the entire period, the reflectances exhibits a strong increase towards one side of the swath (> across-track pixel 300) in the pre-operational Level-1 data before 27 January 2025.

As described in Equation 1), the solar spectral irradiance is the only remaining variable, that can explain differences between radiance and reflectance. In addition to these across-track artifacts, the solar spectral irradiance shows unexpected day-to-day variations of up to 2-3 %.

The artificial across-track behavior was partially mitigated by updating the BSDF for each VNS band, resulting in a smoother reflectance in baseline *AF*. However, it was found out that these BSDF correction factors did not account for seasonal variations,

https://doi.org/10.5194/egusphere-2026-2652
Preprint. Discussion started: 10 June 2026

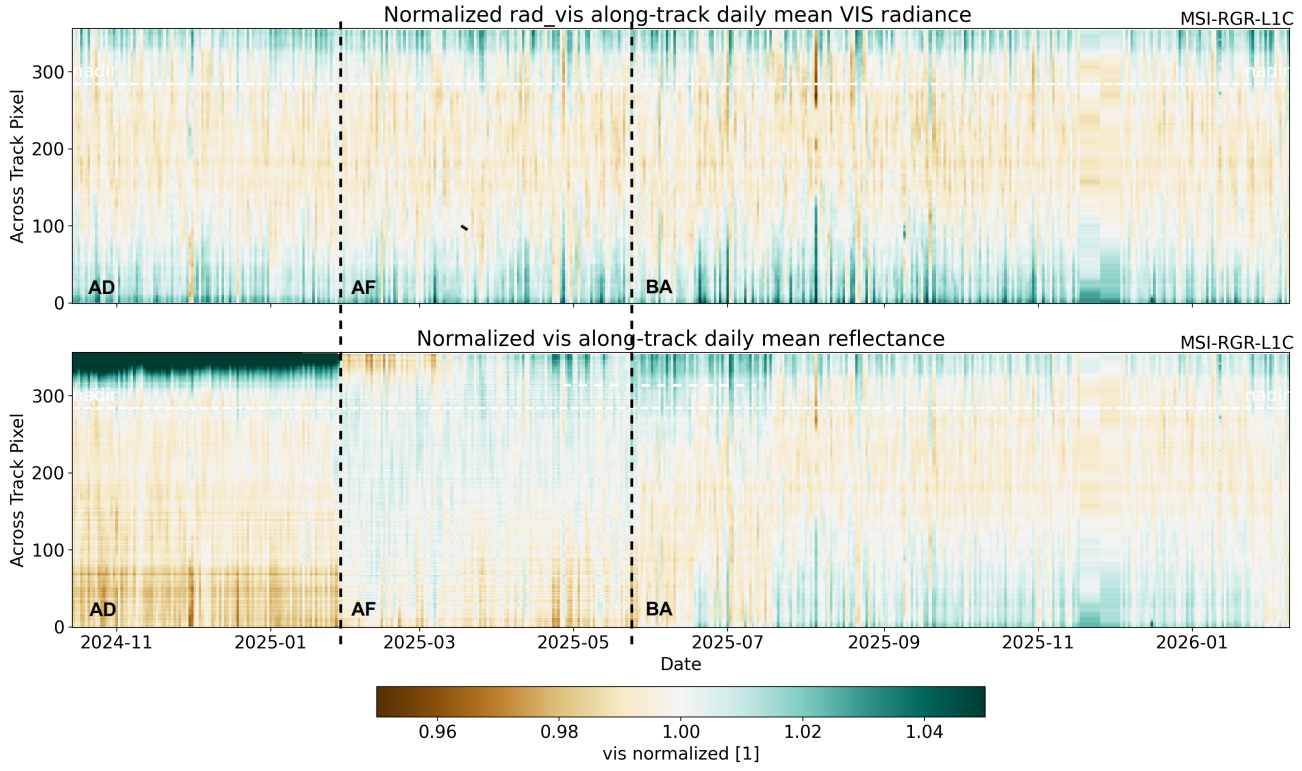

Figure 8. Normalized daily mean radiances (top) and reflectances (bottom), resolved by across-track pixel, for the VIS (0.65 μm) band, covering three different Level-1 product versions.

leading to the decision in June 2025, to replace the measured solar spectral irradiance in the Level-1b (M-NOM) and Level-1c (M-RGR) by theoretical solar spectral irradiance.

They have been calculated for each band by convolving MSI's across-track resolved normalized spectral response functions with a high-resolved solar spectral irradiance (see Fig. B1):

$$I_c = \frac{\int I_\lambda r_{\lambda,c} d\lambda}{\int r_{\lambda,c} d\lambda}, \tag{2}$$

where I_c is the spectral solar irradiance of a MSI band resolved for its across-track pixel c, I_λ is the high-resolved solar spectral irradiance taken from the Total and Spectral Solar Irradiance Sensor-1 Hybrid Solar Reference Spectrum (TSIS-1 HSRS) data base version 2 (Coddington et al., 2023) and $r_{\lambda,c}$ is the normalized MSI response function of a MSI band for each MSI across-track pixel. The resulting solar spectral irradiance for each band can be seen in Figure B2. It is normalized to a sun-Earth distance of 1 AU. However, during the year, this distance varies, and hence the solar spectral irradiance of each MSI band is further scaled with d^{-2}, where d is the actual sun-Earth distance corresponding to the day of the year in AU.

https://doi.org/10.5194/egusphere-2026-2652
Preprint. Discussion started: 10 June 2026

4.2 Ad-hoc vicarious calibration using FCI

FCI Channel	FCI Central λ (μm)	MSI Channel	MSI Central λ (μm)
VIS 0.6	0.640	VIS	0.67
VIS 0.8	0.865	NIR	0.865
NIR 1.6	1.610	SWIR1	1.65
NIR 2.2	2.250	SWIR2	2.21

Table 2. Comparison of MSI and FCI spectral bands and central wavelength.

Given its very similar spectral characteristics (see Table 2) and comparable spatial resolution (MSI 500 m and FCI 1 km), the novel FCI imager onboard MTG is well suited for vicarious calibration of MSI. In addition, its geostationary orbit ensures a sufficient number of collocated observations for each EarthCARE overpass within the MTG full disk. Consequently, FCI was selected for the ad-hoc vicarious calibration of the MSI VNS radiances.

The main limitations of this approach are that it is restricted to collocated observations over the tropics, where viewing geometry differences between MSI and FCI are small, and that, following the ad-hoc vicarious calibration, MSI radiometric performance depends on the absolute radiometric accuracy of FCI. The radiometric performance of FCI is regularly monitored and provided at https://matrics.eumetsat.int/vnir_channels. The VIS06 and VIS08 bands indicate a stable performance with absolute radiometric accuracy of 5 %. The NIR1.6 exhibits seasonal trends up to 5 % which remains unexplained and the NIR2.2 channel shows an offset of 8-12 %.

4.2.1 MSI-FCI Transfer Function

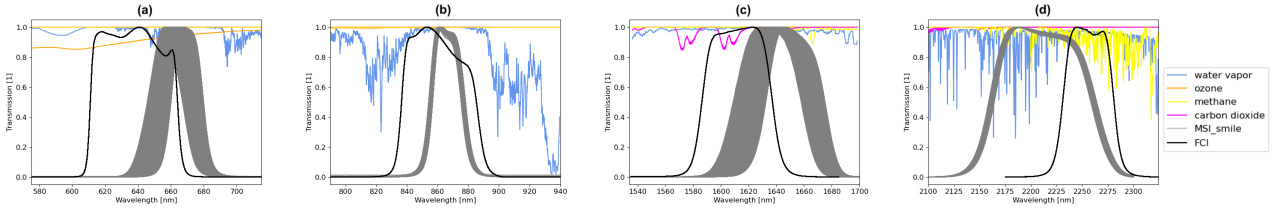

Figure 9. Spectral response functions of MSI, which are across-track resolved, for the a) VIS, b) NIR, c) SWIR-1 and d) SWIR-2 band in grey and of FCI for the a) VIS06, b) VIS08, c) NIR16 and d) NIR22 band in black. Gas transmissions based on the Correlated K-Distribution Model Intercomparison Project (CKDMIP; Hogan and Matricardi (2020)) are shown in coloured lines for water vapour (blue), ozone (orange), methane (yellow) and carbon dioxide (magenta).

For the ad-hoc calibration using FCI data, the MSI and FCI instruments must first be made comparable. We used transfer functions to account for differences in their spectral characteristics (see Fig. 9) and observation geometries before FCI can be reliably used for calibration. We calculated Spectral Band Adjustment Factors (SBAFs) for each band to transfer the FCI

https://doi.org/10.5194/egusphere-2026-2652
Preprint. Discussion started: 10 June 2026

observations to MSI-like observations. This is done by forward simulating MSI- and FCI-like radiances for a variety of different atmospheric conditions and observation geometries. As only cloudy pixels over the ocean are used for the calibration, simulations are performed for cloudy conditions over the ocean only as well. Table 3 shows the different conditions simulated for two liquid and ice clouds. For liquid clouds, an effective radius of 10 μm is used and for ice clouds an effective radius of 30 μm. We have simulated a total of 31590 scenarios for each cloud phase.

Parameter	Values
COT	0, 0.5, 2, 4, 8, 16, 32, 64, 100
CTP [hPa]	200, 500, 800
VZA [°]	0, 5, 10, 15, 20
SZA [°]	10, 15, 20, 25, 30, 35, 40, 45, 50, 55, 60, 65, 70
RAA [°]	0, 10, 20, 30, 40, 50, 60, 70, 80, 90, 100, 110, 120, 130, 140, 150, 160, 170

Table 3. Scenarios used for MORTY-RTS simulations.

For the simulations, we applied the MSI tool, which is based on the Matrix Operator Radiative Transfer in pYthon - Radiative Transfer Solver (Free University Berlin, 2022). Only MSI's nadir pixel is simulated, not taking into account the MSI SMILE effect Docter et al. (2024). Figure C1 shows the resulting MSI-like radiance against FCI-like radiances for the NIR channels (FCI-VIS08/MSI-NIR) and for both cloud phases and all scenarios.

SBAFs are calculated using Eq. 3, where L are the simulated radiances. The resulting SBAFs are displayed in Table 4 and applied to each MSI VNS band for all across-track pixels.

$$SBAF = med\left(\frac{L^{FCI}}{L_{\mathrm{MSI}}}\right) \tag{3}$$

Table 4. Spectral Band Adjustment Factors (SBAFs) for MSI VNS bands to align with FCI spectral response functions.

Band	MSI-VIS / FCI-VIS-06	MSI-NIR / FCI-VIS-08	MSI-SWIR1 / FCI-NIR-16	MSI-SWIR2 / FCI-NIR-22
SBAF	1.045	0.996	1.060	0.925

4.2.2 Cloud Case Selection using FCI

The ad-hoc vicarious calibration is performed using Deep Convective Cloud (DCC) scenes over the tropics. As described in section 4.2, the region of interest is restricted to the southern West African coast and the Gulf of Guinea, near the MTG sub-satellite point, to ensure similar viewing geometries between FCI and MSI. This region, located within the Inter-Tropical Convergence Zone (ITCZ), is characterized by a high DCC frequency. Consequently, only collocated MSI and FCI pixels with sensor zenith angles below 10° were considered. Furthermore, pixel were rejected if the absolute difference between MSI

https://doi.org/10.5194/egusphere-2026-2652
Preprint. Discussion started: 10 June 2026

and FCI viewing angles exceeds 10°. These constraints minimize variations in the observed MSI and FCI radiance due to anisotropic cloud reflectance.

DCC targets are widely used to calibrate passive satellite sensors due to their high and near-invariant reflectance and radiometric stability. Because their cloud tops are typically near the tropopause, their solar reflectance only has a minimal interference with aerosol and atmospheric water vapor.

MSI pixel with a 10.8 μm brightness temperature below 240 K were selected as DCC targets. In previous studies, this threshold was often chosen around 200-210 K (e.g., Doelling et al. (2013)), but we have defined a slightly more relaxed threshold to ensure a sufficient number of data points.

According to these criteria, the following three daytime MSI frames were selected: 03977E (8th February 2025), 03993E (9th February 2025), and 04086E (15th February 2025).

During this short period, FCI showed a stable radiometric performance, expressed as the ratio between the measured and simulated TOA spectral radiances, with values of 0.99 for VIS06, 1.01 for VIS08, 0.98 for NIR1.6, and 0.90 for NIR2.2 (https://matrics.eumetsat.int/vnir_channels).

The collocation between FCI and MSI pixels was performed using a KDTree nearest-neighbor approach applied to the central longitude and latitude of each FCI and MSI pixel. Since MSI provides a higher spatial resolution (500 m) than FCI (1000 m), the nearest FCI pixel was assigned to each MSI pixel. Subsequently, the radiances of all MSI pixels associated with a given FCI pixel were averaged and compared to the radiance of the corresponding FCI pixel. To reduce sub-pixel heterogeneity, only fully cloud-covered FCI pixels (cloud fraction = 1) were retained, based on the M-CM cloud mask product (Hünerbein et al., 2023).

In a second quality control step, a spatial homogeneity filter is applied as described in Doelling et al. (2022, 2025): collocated pixels were discarded if the standard deviation of the MSI NIR radiance within an FCI pixel exceeds 0.1. This filter further reduces the influence of small-scale variability caused by temporal displacements or three-dimensional effects such as radiative enhancement or shadowing at the edge of deep convective clouds (e.g. overshooting cloud tops).

4.2.3 Maintenance Gain Update

After applying the SBAFs to the MSI VNS radiances, selection of DCC cases and quality control according to section 4.2.2, the band-specific calibration gain factors were derived as the slope of the linear regression, while FCI is considered as the reference.

The mean slope obtained from the three DCC scenes was subsequently adopted as a band-specific correction factor. This factor was then applied to the calibrated MSI radiances according to Equation 4.

$$L(MSI)_{\text{corrected}} = c \cdot L(MSI)\text{calibrated} \tag{4}$$

The resulting calibration gain factors are listed in Table 5. They indicate an overestimation of all MSI VNS bands in comparison to the corresponding FCI bands, ranging from approximately 1% for the VIS band to 12% for the SWIR-1 band.

https://doi.org/10.5194/egusphere-2026-2652
Preprint. Discussion started: 10 June 2026

Table 5. Correction factors for the MSI maintenance gains.

Band	MSI-VIS	MSI-NIR	MSI-SWIR1	MSI-SWIR2
Correction factor (c)	0.9596	0.9920	0.8827	0.8970

5 TIR calibration

The three thermal infrared (TIR) bands centered at approximately 8.8 μm, 10.8 μm, and 12.0 μm are radiometrically calibrated using on-board deep-space and blackbody views as cold and warm references, respectively (Chang et al., 2017; Wehr et al., 2023). The MSI Level-1 M-RGR product already provides the calibrated brightness temperatures for each band including measurement uncertainties in Kelvin. Details on the full dataset variables and their definitions can be found in the MSI Level-1 product definition document (MSI, 2025).

The rotating calibration mirror allows to change the view to the deep-space and the blackbody, done once every orbit. These two-point measurements provide detector gain and offset coefficients that are used to convert digital counts to top-of-atmosphere radiances. Next to the Level-0 signal data, the Calibration and Characterization Database (CCDB) is the most important input file for the Level-1 processor. It stores the offset correction and gain factors.

First, a constant TIR display offset, stored in the CCDB, is subtracted from each column in every measured line for each of the three TIR bands (Eisinger et al., 2024).

After column correction, the radiometric calibration of the MSI TIR channels is performed using a two-step approach: (a) removal of an offset associated with the cold space mirror emissivity, and (b) application of a gain factor to convert the TIR signals into brightness temperatures. While daily deep-space (for offset characterization) and blackbody measurements (for gain assessment) allow regular characterization of these parameters, initial configuration of the MSI Level 1 processor relies exclusively on pre-flight offset and gain coefficients. Daily offset and gain measurement statistics are monitored offline and if drifts are detected, the offset and gain factors applied during the calibration process will be updated accordingly.

Radiometric calibration processing also includes sensitivity correction for small perturbations. Indeed, the sensitivity of the calibration has been characterized on-ground with respect to the perturbations of parameters such as the temperatures of various elements of the TIR camera or the voltage settings of the detectors. Control systems maintain these parameters within a nominal range. Nevertheless, these parameters are monitored via ancillary telemetry, and in case of unacceptable deviation, additional sensitivity correction of offset and gain values would be activated in the processing chain.

During the commissioning phase, a small offset was detected in the TIR-3 brightness temperatures compared to corresponding bands of FCI. The deviation was small and became evident only through brightness temperature differences (e.g., TIR-2 - TIR-3) relative to the other sensors. Although minor, such discrepancies in temperature differences can significantly affect the performance of the M-CM cloud mask algorithm, which relies on accurate thermal contrast information. Detailed analysis traced the source of the offset to the TIR-3 band calibration. After correction of column-specific gain factors, the absolute differences with respect to the corresponding FCI bands were reduced to less than 1 K.

https://doi.org/10.5194/egusphere-2026-2652
Preprint. Discussion started: 10 June 2026

Also, during the commissioning phase, apparent TIR bands striping (i.e. across-track oscillations) were addressed by manually updating the pixel-resolved maintenance gain values. These coefficients have been derived by comparing the calibrated brightness temperatures derived from internal blackbody measurement to temperatures measured by the blackbody temperature sensors.

6 Results

During the first one and a half years of MSI operation, the data products have already demonstrated their capability to provide valuable contextual information at 500 m resolution. For example, on 7 February 2025, when EarthCARE captured Tropical Cyclone Vince, the nadir track passed almost directly through the eye of the storm (ESA EarthCARE DISC Team, 2025). Scenes like that, enabling for the first time direct connections between cloud top properties and vertically resolved cloud dynamics, demonstrate the great potential of EarthCARE with its synergistic instruments.

In addition, the first fully reprocessed baseline *BA* MSI Level-1 dataset provides a radiometric stable and consistent dataset of more than one and a half years, including geolocation and coregistration corrections as well as radiometric calibration updates through ad-hoc vicarious calibration.

6.1 Global statistics

The average brightness and temperature of the Earth, measured by MSI in June 2025, is presented in Figure 10. It shows monthly mean VIS reflectance and TIR-2 band brightness temperature (K), averaged at 0.1° resolution. The latitudinal coverage of MSI is limited to approximately 84°N to 84°S, which is due to the inclination of the EarthCARE sun-synchronous orbit of 97°. The monthly mean VIS reflectance is cut around 60°S, because data with solar zenith angle larger than 80° is excluded from the average.

Because it is NH summer, the Arctic is relatively warm, while minimum temperatures are observed over the Antarctic and around the equator, where deep convective clouds frequently occur in the Intertropical Convergence Zone (ITCZ). The maximum brightness temperatures are found over the Sahara, the Arabian Peninsula and around the golf of California. Apart from the snow and ice area in the Arctic, the brightest spots are at cloud tops and over desert areas. It is remarkable how bright the mean reflectance is over Central America, demonstrating the strong dominance of deep convective clouds.

Figure 11 shows the frame-mean reflectance for the VIS band and the brightness temperature for the TIR-3 band for each of the eight frames covering the period from October 2024 to November 2025. The time series reveal a clear seasonal cycle for the Arctic (Frame *C*) and Antarctic (Frame *G*), both in reflectance and brightness temperature. In both regions, the values are high during the respective hemispheric summer and low during winter. An interesting feature is that, while the Antarctic exhibits a sinusoidal seasonal variation that closely follows the solar zenith angle, the reflectance over the Arctic shows an almost linear increase towards mid-June and a subsequent linear decrease to near zero in November.

The linear increase and subsequent decrease of reflectance in the Arctic is likely caused by a complex interplay of increasing solar irradiance, sea-ice decline, enhanced open-water areas, and cloud–surface–albedo feedbacks. The fact that the reflectance

https://doi.org/10.5194/egusphere-2026-2652
Preprint. Discussion started: 10 June 2026

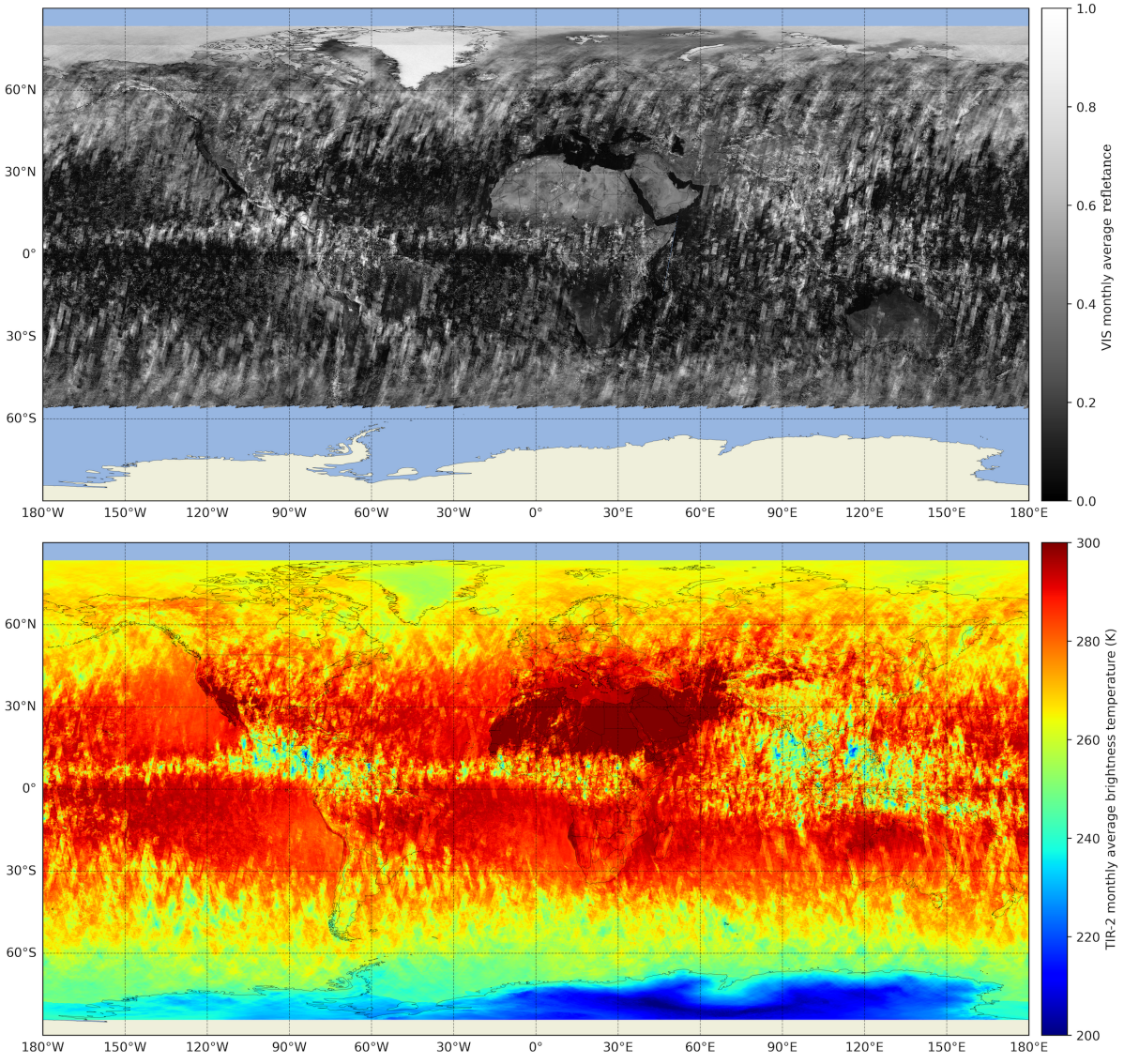

Figure 10. Top: Monthly mean VIS reflectance at 0.1° resolution for June 2025 (excluding data with solar zenith angle > 80°). Bottom: Monthly mean brightness temperature (K) for the TIR-2 band at 0.1° resolution for June 2025 (all data included).

starts to decrease already before the peak in incoming solar radiation around the summer solstice (in contrast to Frame *B*, where the peak reflectance is equal to the summer solstice) strongly suggests that this behavior is driven by the reduction in sea-ice extent and the associated decrease in surface albedo. Perovich and Polashenski (2012) reported a rapid and nearly linear decrease in the surface albedo over the Arctic beginning around 1 June, which is consistent with our observations for Frame *C*. However, the decline in reflectance is less steep than the decrease in surface albedo, indicating a potential

https://doi.org/10.5194/egusphere-2026-2652
Preprint. Discussion started: 10 June 2026

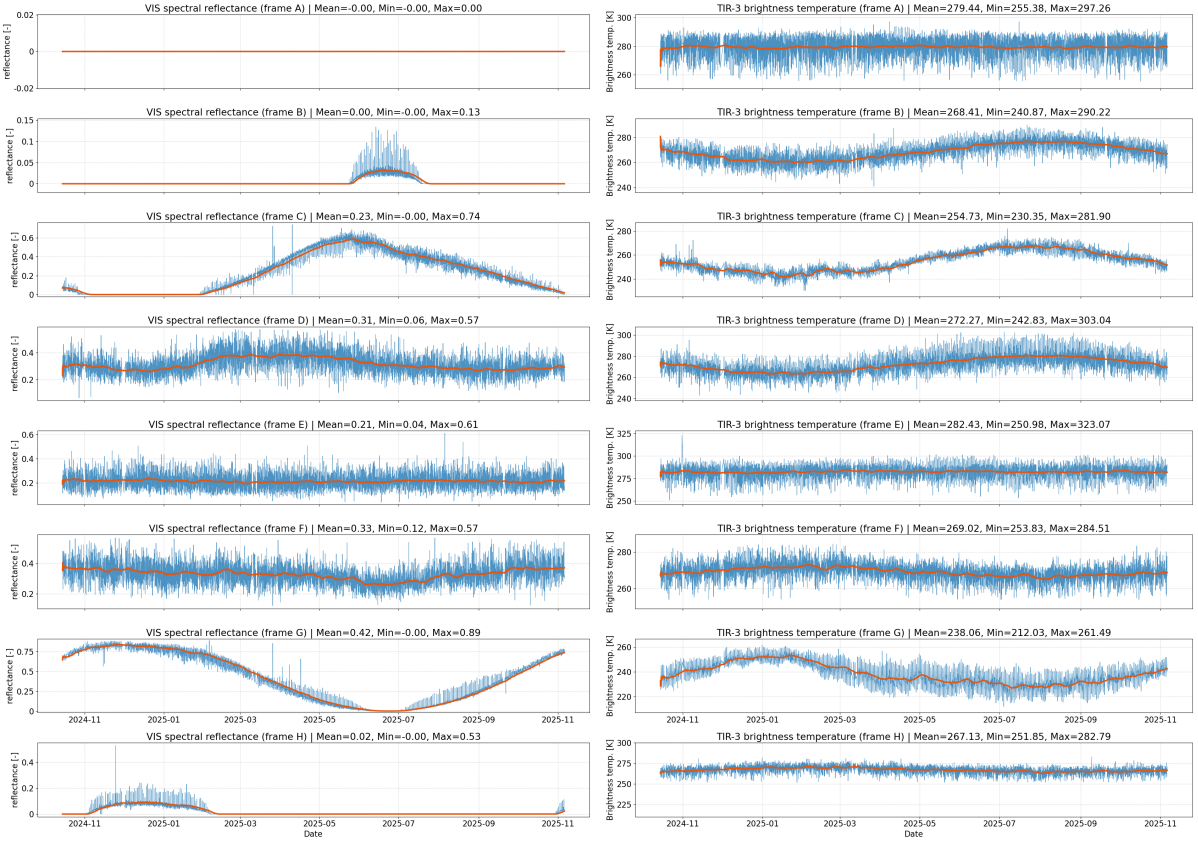

Figure 11. Frame-mean VIS reflectance (left) and TIR-3 brightness temperature (right) from M-RGR Level-1 baseline **BA** data. About 15 frame-mean values per day are shown for each frame. The red line shows the 7-day running mean. Sub-figure titles list the mean, minimum, and maximum for each frame-mean time series.

compensating effect from clouds. Eastman and Warren (2010) found that the cloud fraction over the Arctic peaks between July and September, which could explain the slower decline in TOA reflectance during summer. This interpretation is further supported by Barrientos-Velasco et al. (2025), who showed that the cloud radiative effect in the Arctic is strongly modulated by changes in cloud optical properties and surface albedo, with the strongest modulation occurring during the summer months (June to August).

In contrast, the Antarctic surface retains a more persistent ice/snow cover with fewer transitions to open water, so the reflectance time series has a more sinusoidal seasonal cycle.

Frames *B* and *H* are the Northern and Southern Hemisphere night frames with a reflectance of close to zero for most of the time, expect of the two summer months when the sun illuminates large parts of the high latitudes. Frames *D* and *F* are the day-time counterparts, showing only a small seasonal cycle, while the seasonal cycle of the brightness temperature is a bit

https://doi.org/10.5194/egusphere-2026-2652
Preprint. Discussion started: 10 June 2026

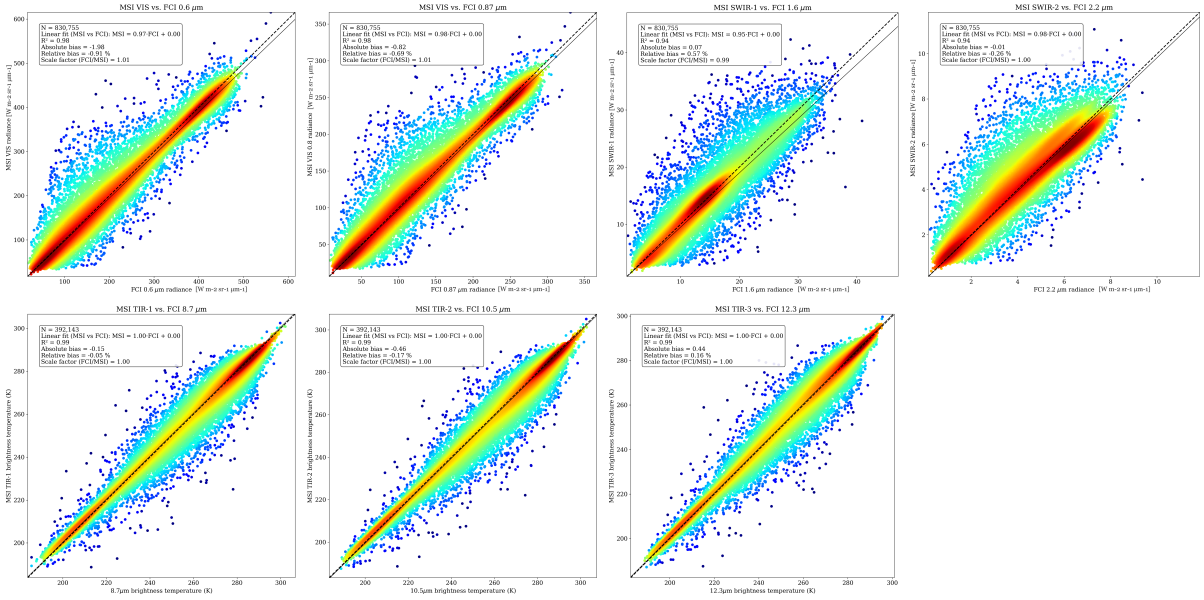

Figure 12. Density scatter plots for the comparison between MSI Level-1c (baseline *BA*) and FCI Level-1c VNS radiances (top row) and TIR brightness temperatures (bottom row) from 25 collocated scenes between April and August 2025 for cloudy pixel applying the same QC as described in section 4.2.

more pronounced for frame *D* due to the higher land coverage of the NH compared to the SH. The tropical frames *E* and *A* show no seasonal cycle and the mean brightness temperatures is almost identical between day and night.

6.2 Verification against FCI

Figure 12 shows the intercomparison between collocated MSI Level-1 M-RGR (baseline *BA*) and FCI Level-1c radiances and brightness temperatures, based on 25 collocated scenes between April and August 2025 for EarthCARE frames *E*. In total, approximately 830.000 pixel were used for VNS bands and 392.000 pixel for the TIR bands, applying the same quality criteria as described in section 4.2. The number of VNS pixels is roughly twice that of the TIR pixels because the FCI TIR channels have a spatial resolution of 2 km, compared to 1 km for the FCI VIS bands. Since FCI pixels were excluded from the comparison whenever the sub-pixel MSI cloud fraction was smaller than 1, as indicated by the MSI M-CM cloud mask, the total number of TIR pixels is consequently less than half the number of VNS pixels.

The scatter density plots show a good agreement between the two instruments across all MSI spectral bands. The correlation coefficient (R^2) reaches 0.98 for the VIS and NIR bands and 0.94 for the SWIR-1 and SWIR-2 bands. The relative bias remains below 1% for all VNS bands, demonstrating the successful removal of discrepancies between MSI and FCI radiances by applying ad-hoc vicarious calibration for DCC scenes.

The spread in the VNS scatter plots is noticeably larger than in the TIR plots. This suggests that cloud displacement due to the small temporal offset between the MSI and FCI observations is minor, whereas three-dimensional cloud effects become

https://doi.org/10.5194/egusphere-2026-2652
Preprint. Discussion started: 10 June 2026

visible in the VNS bands because of the imperfectly matched viewing geometries. Even when limiting the absolute viewing-angle differences between the two sensors to less than 10°, variations in illumination and shadowing at cloud edges can still introduce significant differences in the measured spectral radiances.

The spread in the SWIR-1 and SWIR-2 scatter plots is larger than in the VIS and NIR bands, consistent with their lower R^2. This can likely be attributed to two main factors: (1) limitations in the computation of the SBAFs and (2) a higher temporal radiometric instability in the corresponding short-wave infrared FCI bands (see https://matrics.eumetsat.int/vnir_channels). The first point relates to the use of fixed cloud droplet and ice crystal effective radii in the FCI and MSI simulations, whereas only the cloud optical thickness was varied for both, ice and water clouds (see Section 4.2.1). While the VIS and NIR bands are primarily sensitive to cloud optical thickness, the SWIR-1 and SWIR-2 bands are strongly affected by absorption from cloud droplets and ice crystals and therefore depend more directly on the effective radius. Consequently, we expect greater deviations between the FCI and MSI SWIR bands as cloud microphysical properties vary.

The brightness temperatures of the MSI TIR bands show excellent agreement with the corresponding FCI bands. Absolute deviations are below 0.5 K for all three bands, demonstrating the robustness of the MSI TIR calibration. Even for very cold cloud tops around 200 K, the agreement remains outstanding, indicating that the thermal noise of the MSI TIR bands is small even for low signals.

7 Conclusions

We have presented an overview of the first one and a half years of EarthCARE MSI Level-1 data, which has been fully reprocessed using the Level-1 processor version baseline *BA* covering 16 July 2024 until now (including baseline *BC*). This baseline includes several major updates: corrections of the MSI pixel geolocation and coregistration, replacement of the measured solar spectral irradiance by theoretical values, an ad-hoc vicarious calibration of the VNS radiances using data from the FCI imager onboard MTG and an update of the calibration gains for the TIR-3 band. These updates led to a significant improvement in the radiometric and geometric stability of the MSI Level-1 product, as shown in this article.

The assessment of MSI Level-1b pixel registration and Level-1c band-to-band coregistration showed that the initial dataset did not meet the mission requirements. The corrections implemented within baseline *BA* led to a geolocation and coregistration accuracy of 500 m and 0.3 pixel, respectively, which is within the mission requirements. This accuracy can change over time and depending on the orbital position. Therefore, continuous monitoring throughout the entire mission is required to ensure a stable geolocation and coregistration performance.

The ad-hoc vicarious calibration is based on three deep convective cloud scenes in the tropics, for which MSI VNS radiances were compared to corresponding FCI bands through an adjustment of the MSI spectral bands using spectral band adjustment factors (SBAFs) to match the FCI response functions. The SBAFs were derived using radiative transfer simulations for nadir pixels only, and therefore do not account for the SMILE effect. In addition, the simulations cover a limited range of cloud microphysics, with varying optical thicknesses for ice and water clouds but with fixed effective radii for each cloud class. This

https://doi.org/10.5194/egusphere-2026-2652
Preprint. Discussion started: 10 June 2026

could cause uncertainties for highly absorbing clouds, such as ice clouds, and consequently can result in uncertainties for both SWIR-1 and SWIR-2 bands.

The replacement of the measured solar spectral irradiance in the MSI Level-1c product by theoretical values achieved temporal radiometric stability, which is an essential prerequisite for ad-hoc vicarious calibration. However, further characterization of the diffuser measurements is required for monitoring of instrument degradations.

Verification of the reprocessed MSI Level-1 baseline *BA* dataset was performed using 25 additional DCC scenes from FCI between April and August 2025. Those FCI scenes were chosen, which show a comparable radiometric performance to the three scenes used for the ad-hoc vicarious calibration in February 2025. Consequently, a reasonable level of agreement is expected and this verification serves as consistency check for the calibration method. The verification shows a good agreement between the two instruments for all MSI bands with remaining biases smaller than 1% relative to FCI. It should be noted, that this ad-hoc vicarious calibration relies on the radiometric performance of FCI, which is varying especially for the SWIR-1 band. The EUMETSAT MATRICS instrument monitoring tool provides regular assessment of the radiometric accuracy of FCI (https://matrics.eumetsat.int/vnir_channels). During the time of the MSI ad-hoc vicarious calibration (February 2025), it shows a very good performance for the VIS and NIR channel, but an underestimation of 2-3% for the SWIR-1 and 10% for the SWIR-2 band.

ESA has recently initiated a new operational service called VICALOPS, which is designed to perform vicarious radiometric calibration of multiple satellite sensors (Berthelot et al., 2024). VICALOPS already includes missions such as MODIS, SLSTR, VIIRS, OLCI, Sentinel-2, and is currently also analyzing MSI Level-1 data from baseline *BA* for different calibration sites. This work is ongoing.

The first ad-hoc vicarious calibration, presented in this article, enabled an immediate improvement of the Level-1 data and is a prerequisite for future comprehensive vicarious calibration activities, such as VICALOPS. The resulting MSI Level-1 baseline *BA*, generated within the first full-mission reprocessing, offers a geometrically and radiometrically stable dataset, covering the first one and a half years of the mission.

Regardless of the outcome of the ongoing diffuser investigations, continuous vicarious calibration is required throughout the entire mission to ensure a stable radiometric performance. This should include more calibration targets in addition to DCC scenes, more geographical locations and longer time periods.

Additionally, more reference measurements are needed (e.g., airborne imagers, other satellite imagers) for independent Level-1 product validation. Although the current analysis is limited to 10° around the MSI nadir pixel, we should extend the validation activities to the full swath and include hyperspectral imagers to better quantify across-track uncertainties and the impact of the SMILE effect. In addition, the influence of three-dimensional radiative effects, particularly for very high reflectance values, should be assessed.

Future work shall include vertically resolved measurements from the active CPR and ATLID instruments to better understand uncertainties in the MSI observations and the corresponding aerosol and cloud retrievals.

https://doi.org/10.5194/egusphere-2026-2652
Preprint. Discussion started: 10 June 2026

Data availability. The EarthCARE data is available at ESA's MAAP (Multi-mission Algorithm and Analysis Platform, https://portal.maap.eo.esa.int/). Level-1c data from the FCI onboard MTG is publicly available through the EUMETSAT data portal (https://data.eumetsat.int/data/map/EO:EUM:DAT:0662)

Code and data availability. Figure 1 was created using the earthcarekit (König et al., 2025): https://pypi.org/project/earthcarekit/ Many more EarthCARE products can be visualized with this software package. The MSI-FCI transfer function was calculated using the MSI tool (Free University Berlin, 2022): https://gitlab.com/wew_fub/msi-tool.

Author contributions. All authors have contributed to this work. SB and AH conceptualized the ad-hoc vicarious calibration and validation against FCI and wrote the manuscript together with EB, NM and ND. ED analyzed the geolocation and coregistration performance and drafted the corresponding section. NM and RP developed the MSI-FCI transfer function through MORTY-RTS and wrote the section about it. ND calculated the theoretical solar irradiance and drafted the associated section. MR, CB, FM and SA implemented all updates in the operational Level-1 processor and revised the processor description. ME, FM and LZ supported the development of the Level-1 processor and contributed to the implementation of the calibration gain factors. AL and TH provided suggestions for the processor updates and enabled the exchange between the instrument & processor developers with the EarthCARE DISC team.

Competing interests. The authors declare that they have no conflict of interest.

Disclaimer. The present work includes preliminary MSI Level-1 data (not fully calibrated/validated and not yet publicly released) of the EarthCARE ESA mission developed in collaboration with JAXA. The analysis has been performed in the context MSI Integrated Commissioning Team, MSI instrument working group, the EarthCARE Data Innovation & Science Cluster (DISC) and the EarthCARE Validation project GIVE.

Acknowledgements. The work has been carried out primarily in the framework of the CARDINAL project (Clouds, Aerosol, Radiation - Development of INtegrated ALgorithms) for the EarthCARE Mission (TROPOS to ESA Contract No. 4000134661/21/NL/AD), the EarthCARE Data Innovation & Science Cluster (DISC) under ESA Contract No. 4000144997/24/I-NS and in the framework of the German Initiative for the Validation of EarthCARE (GIVE) funded by the German Federal Ministry for Economic Affairs and Energy (BMWE, grant no. 50EE2403A). We thank Tobias Wehr and Michael Eisinger for their continuous support over many years, and the EarthCARE developer team for valuable discussions during various meetings. We also thank the entire MSI commissioning team and instrument working group for contributing to all the MSI investigations since launch and Airbus for supporting these investigations and for providing valuable input regarding instrument and raw data issues. We are grateful for the fruitful discussions and exchanges about MSI Level-1 validation and calibration with the JAXA and Tokai University EarthCARE MSI team. We also thank Ali Mousivand and Alessio Bozzo from EUMETSAT for their

https://doi.org/10.5194/egusphere-2026-2652
Preprint. Discussion started: 10 June 2026

valuable suggestions regarding the FCI radiometric performance and vicarious calibration methods. The authors used deepL and Grammarly to improve grammar in some parts of the text.

https://doi.org/10.5194/egusphere-2026-2652
Preprint. Discussion started: 10 June 2026

A Geolocation and coregistration assessment

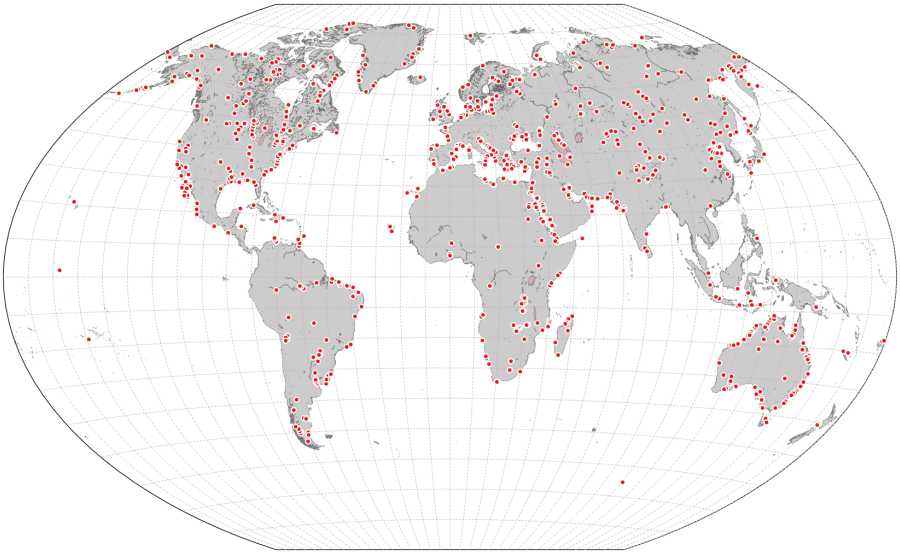

Figure A1. Global distribution of scenes for geolocation and coregistration assessment, described in sections 3.1 and 3.2.

B Theoretical Solar Spectral Irradiance

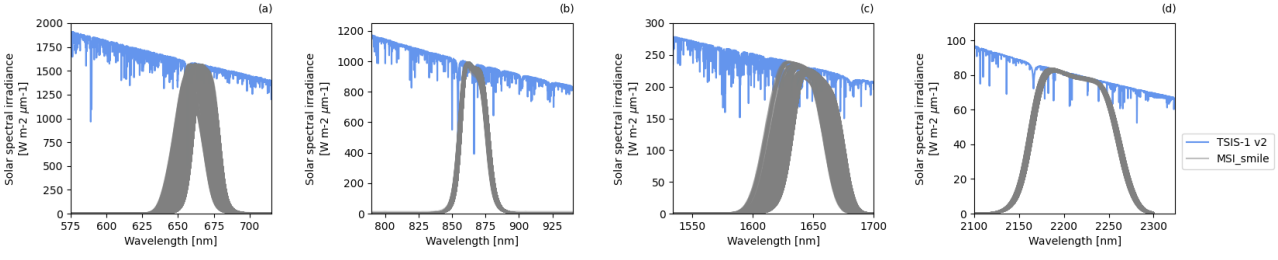

Figure B1. Scaled spectral response functions of MSI in grey and TSIS-1 HSRS in blue.

https://doi.org/10.5194/egusphere-2026-2652
Preprint. Discussion started: 10 June 2026

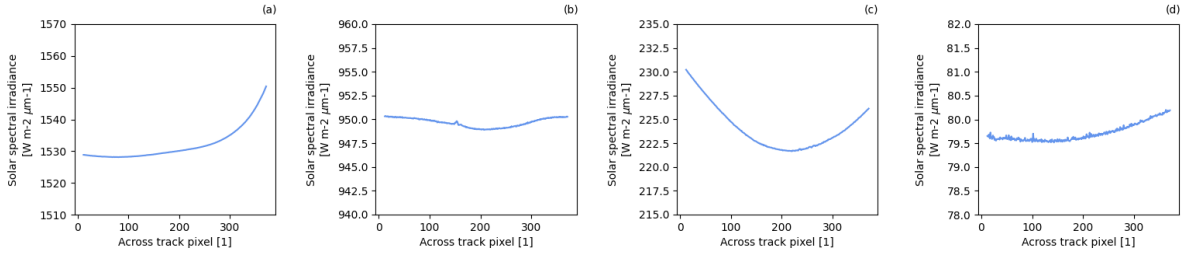

Figure B2. MSI spectral solar irradiance for a reference sun-Earth distance of 1 AU.

C MSI-FCI Transfer Functions

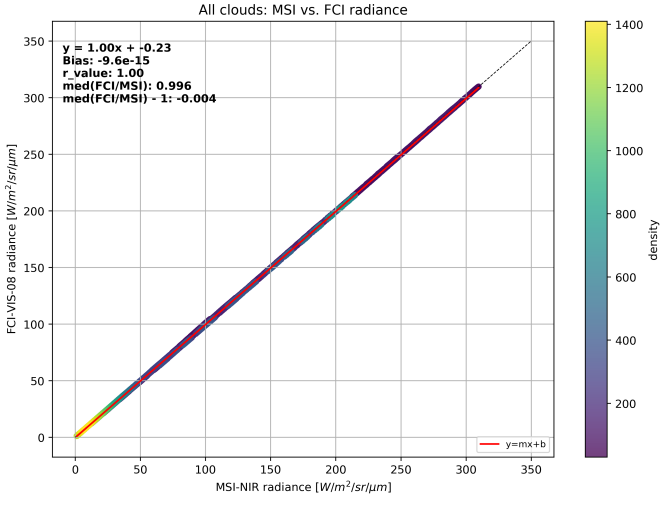

Figure C1. Density plot of simulated FCI-VIS08- and MSI-NIR-like radiances for all scenarios and both cloud phases.

https://doi.org/10.5194/egusphere-2026-2652
Preprint. Discussion started: 10 June 2026

References

MSI L1 PRODUCT DEFINITIONS, GMV, https://earthcarehandbook.earth.esa.int/documents/d/earthcare-data-handbook/msi-l1-%20product-definitions-volume-a-nominal-products, 2025.

Airbus Defence and Space GmbH.: Copernicus Digital Elevation Model Product Handbook, https://doi.org/10.5270/ESA-c5d3d65, 2022.

Albinana, A. P., Gelsthorpe, R., Lefebvre, A., Sauer, M., Kruse, K.-W., Münzenmayer, R., Baister, G., and Chang, M.: The calibration of the multi-spectral imager on-board the EarthCARE spacecraft, in: Infrared Remote Sensing and Instrumentation XIX, edited by Strojnik, M. and Paez, G., vol. 8154, p. 81540D, International Society for Optics and Photonics, SPIE, https://doi.org/10.1117/12.891903, 2011.

Barrientos-Velasco, C., Cox, C. J., Deneke, H., Dodson, J. B., Hünerbein, A., Shupe, M. D., Taylor, P. C., and Macke, A.: Estimation of the radiation budget during MOSAiC based on ground-based and satellite remote sensing observations, Atmospheric Chemistry and Physics, 25, 3929–3960, https://doi.org/10.5194/acp-25-3929-2025, 2025.

Berthelot, B., Fassot, G., Lalanne, T., Sainte-Marie, L., De Vis, P., Zimmerman, A., and Bouvet, M.: VICALOPS: Operational Service for Vicarious Calibration, Presentation at the VH-RODA 2024 Workshop, ESA-ESRIN, Frascati, Italy, https://earth.esa.int/eogateway/documents/d/earth-online/8_bberthelot_magellium, accessed: 2026-02-06, 2024.

Bouvet, M.: Radiometric comparison of multispectral imagers over a pseudo-invariant calibration site using a reference radiometric model, Remote sensing of environment, 140, 141–154, 2014.

Cao, C., Xiong, J., Blonski, S., Liu, Q., Uprety, S., Shao, X., Bai, Y., and Weng, F.: Suomi NPP VIIRS sensor data record verification, validation, and long-term performance monitoring, Journal of Geophysical Research: Atmospheres, 118, 11,664–11,678, https://doi.org/https://doi.org/10.1002/2013JD020418, 2013.

Cao, C., De Luccia, F. J., Xiong, X., Wolfe, R., and Weng, F.: Early On-Orbit Performance of the Visible Infrared Imaging Radiometer Suite Onboard the Suomi National Polar-Orbiting Partnership (S-NPP) Satellite, IEEE Transactions on Geoscience and Remote Sensing, 52, 1142–1156, https://doi.org/10.1109/TGRS.2013.2247768, 2014.

Chang, M. P. J. L., Woods, D., Baister, G., Lobb, D., and Wood, T.: The EarthCARE multi spectral imager thermal infrared optical unit, in: International Conference on Space Optics — ICSO 2010, edited by Armandillo, E., Cugny, B., and Karafolas, N., vol. 10565, p. 105651T, International Society for Optics and Photonics, SPIE, https://doi.org/10.1117/12.2309143, 2017.

Coddington, O. M., Richard, E. C., Harber, D., Pilewskie, P., Woods, T. N., Snow, M., Chance, K., Liu, X., and Sun, K.: Version 2 of the TSIS-1 Hybrid Solar Reference Spectrum and Extension to the Full Spectrum, Earth and Space Science, 10, e2022EA002 637, https://doi.org/https://doi.org/10.1029/2022EA002637, 2023.

de Goeij, B. T. G., de Bruijn, D., van der Knaap, F., Bol, H., Gielesen, W., Bell, A., Matthews, A., Skipper, M., Hallett, B., Sauer, M., Kruse, K.-W., Haas, C., Wallace, K., and Heliere, A.: Characterisation and performance verification results of the EarthCARE multi spectral imager VNS camera, in: International Conference on Space Optics — ICSO 2018, edited by Sodnik, Z., Karafolas, N., and Cugny, B., vol. 11180, p. 111804I, International Society for Optics and Photonics, SPIE, https://doi.org/10.1117/12.2536081, 2019.

de Vries, C., Danaher, T., Denham, R., Scarth, P., and Phinn, S.: An operational radiometric calibration procedure for the Landsat sensors based on pseudo-invariant target sites, Remote Sensing of Environment, 107, 414–429, https://doi.org/https://doi.org/10.1016/j.rse.2006.09.019, 2007.

Docter, N., Preusker, R., Filipitsch, F., Kritten, L., Schmidt, F., and Fischer, J.: Aerosol optical depth retrieval from the EarthCARE Multi-Spectral Imager: the M-AOT product, Atmospheric Measurement Techniques, 16, 3437–3457, https://doi.org/10.5194/amt-16-3437-2023, 2023.

https://doi.org/10.5194/egusphere-2026-2652
Preprint. Discussion started: 10 June 2026

Docter, N., Hünerbein, A., Donovan, D. P., Preusker, R., Fischer, J., Meirink, J. F., Stammes, P., and Eisinger, M.: Assessment of the spectral misalignment effect (SMILE) on EarthCARE's Multi-Spectral Imager aerosol and cloud property retrievals, Atmospheric Measurement Techniques, 17, 2507–2519, https://doi.org/10.5194/amt-17-2507-2024, 2024.

Doelling, D., Khakurel, P., Haney, C., Gopalan, A., and Bhatt, R.: Regional Characterization of Deep Convective Clouds for Enhanced Imager Stability Monitoring and Methodology Validation, Remote Sensing, 17, https://doi.org/10.3390/rs17183258, 2025.

Doelling, D. R., Morstad, D., Scarino, B. R., Bhatt, R., and Gopalan, A.: The Characterization of Deep Convective Clouds as an Invariant Calibration Target and as a Visible Calibration Technique, IEEE Transactions on Geoscience and Remote Sensing, 51, 1147–1159, https://doi.org/10.1109/TGRS.2012.2225066, 2013.

Doelling, D. R., Haney, C., Bhatt, R., Scarino, B., and Gopalan, A.: Daily monitoring algorithms to detect geostationary imager visible radiance anomalies, Journal of Applied Remote Sensing, 16, 014 502, https://doi.org/10.1117/1.JRS.16.014502, 2022.

Eastman, R. and Warren, S. G.: Interannual Variations of Arctic Cloud Types in Relation to Sea Ice, Journal of Climate, 23, 4216 – 4232, https://doi.org/10.1175/2010JCLI3492.1, 2010.

Eisinger, M., Marnas, F., Wallace, K., Kubota, T., Tomiyama, N., Ohno, Y., Tanaka, T., Tomita, E., Wehr, T., and Bernaerts, D.: The EarthCARE mission: science data processing chain overview, Atmospheric Measurement Techniques, 17, 839–862, https://doi.org/10.5194/amt-17-839-2024, 2024.

ESA EarthCARE DISC Team: EarthCARE stares into the eye of Tropical Cyclone Vince, https://earth.esa.int/eogateway/success-story/earthcare-stares-into-the-eye-of-tropical-cyclone-vince, 2025.

ESA EarthCARE Mission Team: EarthCARE Product Disclaimer – MSI Level 1, https://earthcarehandbook.earth.esa.int/documents/d/earthcare-data-handbook/earthcare-msi-level-1-product-disclaimer, 2025.

ESA EarthCARE Team: EarthCARE Product Definition and Format, https://earthcarehandbook.earth.esa.int/article/product, 2025.

European Space Agency: Database for Imaging Multi-spectral Instruments and Tools for Radiometric Intercomparison (DIMITRI), https://dimitri.argans.co.uk, 2016.

European Space Agency: EarthCARE lifetime update: mission targets 2034 and beyond, https://earth.esa.int/eogateway/news/earthcare-lifetime-update-mission-targets-2034-and-beyond, 2025.

Free University Berlin: MSI-tool, https://gitlab.com/wew_fub/msi-tool, gitLab repository, last access: 27 March 2026, 2022.

Helder, D., Thome, K. J., Mishra, N., Chander, G., Xiong, X., Angal, A., and Choi, T.: Absolute Radiometric Calibration of Landsat Using a Pseudo Invariant Calibration Site, IEEE Transactions on Geoscience and Remote Sensing, 51, 1360–1369, https://doi.org/10.1109/TGRS.2013.2243738, 2013.

Hogan, R. J. and Matricardi, M.: Evaluating and improving the treatment of gases in radiation schemes: the Correlated K-Distribution Model Intercomparison Project (CKDMIP), Geoscientific Model Development, 13, 6501–6521, https://doi.org/10.5194/gmd-13-6501-2020, 2020.

Hünerbein, A., Bley, S., Horn, S., Deneke, H., and Walther, A.: Cloud mask algorithm from the EarthCARE Multi-Spectral Imager: the M-CM products, Atmospheric Measurement Techniques, 16, 2821–2836, https://doi.org/10.5194/amt-16-2821-2023, 2023.

Hünerbein, A., Bley, S., Deneke, H., Meirink, J. F., van Zadelhoff, G.-J., and Walther, A.: Cloud optical and physical properties retrieval from EarthCARE multi-spectral imager: the M-COP products, Atmospheric Measurement Techniques, 17, 261–276, https://doi.org/10.5194/amt-17-261-2024, 2024.

Japan Aerospace Exploration Agency: EarthCARE/MSI L2A MSI one-sensor Cloud Products, https://doi.org/10.57746/EO.01jkwjkd9yt4shyz0z27drfve3, 2024.

https://doi.org/10.5194/egusphere-2026-2652
Preprint. Discussion started: 10 June 2026

Khadka, N., Teixeira Pinto, C., and Leigh, L.: Detection of Change Points in Pseudo-Invariant Calibration Sites Time Series Using Multi-Sensor Satellite Imagery, Remote Sensing, 13, https://doi.org/10.3390/rs13112079, 2021.

König, L., Floutsi, A. A., Haarig, M., Baars, H., Mason, S., and Wandinger, U.: earthcarekit: A Python package to simplify working with EarthCARE satellite data, https://doi.org/10.5281/zenodo.16813294, 2025.

Le Moigne, J., Netanyahu, N. S., and Eastman, R. D.: Image Registration for Remote Sensing, Cambridge University Press, 2011.

Lobb, D., Escadero, I., Chang, M., and Gode, S.: Development of detailed design concepts for the EarthCARE multi-spectral imager, in: International Conference on Space Optics—ICSO 2008, vol. 10566, pp. 116–123, SPIE, 2017.

Mousivand, A., Straif, C., Burini, A., Lekouara, M., Debaecker, V., Hewison, T., Stock, S., and Bojkov, B.: In-Flight Calibration of Geostationary Meteorological Imagers Using Alternative Methods: MTG-I1 FCI Case Study, Remote Sensing, 17, https://doi.org/10.3390/rs17142369, 2025.

Perovich, D. K. and Polashenski, C.: Albedo evolution of seasonal Arctic sea ice, Geophysical Research Letters, 39, https://doi.org/https://doi.org/10.1029/2012GL051432, 2012.

Rayference: Development of a deep convective cloud reference model for vicarious calibration, EUMETSAT, https://www.eumetsat.int/media/42131, 2017.

Tabak, E., de Goeij, B., van Riel, L., Meijer, E., van der Knaap, F., Doornink, J., and de Graaf, H.-J.: Design, building and testing of a Sun calibration mechanism for the MSI-VNS instrument on Earthcare, in: Conference proceedings of the 15th European Space Mechanisms & Tribology Symposium, 1, pp. 25–27, ESA 25–27 September, Noordwijk, The Netherlands, 2013.

Team, J. E.: EarthCARE/CPR Level 1b Product Definition Document, https://earth.esa.int/eogateway/documents/20142/37627/EarthCARE-CPR-L1B-PDD.pdf.

Wehr, Tobias, e.: EarthCARE Mission Requirements Document, Earth and Mission Science Division, European Space Agency, https://doi.org/https://doi.org/10.5270/esa.earthcare-mrd.2006, 2006.

Wehr, T., Kubota, T., Tzeremes, G., Wallace, K., Nakatsuka, H., Ohno, Y., Koopman, R., Rusli, S., Kikuchi, M., Eisinger, M., Tanaka, T., Taga, M., Deghaye, P., Tomita, E., and Bernaerts, D.: The EarthCARE mission – science and system overview, Atmospheric Measurement Techniques, 16, 3581–3608, https://doi.org/10.5194/amt-16-3581-2023, 2023.

Xiong, X., Angal, A., Twedt, K. A., Chen, H., Link, D., Geng, X., Aldoretta, E., and Mu, Q.: MODIS reflective solar bands on-orbit calibration and performance, IEEE Transactions on Geoscience and Remote Sensing, 57, 6355–6371, 2019.

Zimmermann, L., Haas, C., Canas, T., Ghose, K., Wallace, K., Kruse, K., and Sauer, M.: MSI (Multi Spectral Imager) performance check at integrated EarthCARE satellite system, in: International Conference on Space Optics — ICSO 2022, edited by Minoglou, K., Karafolas, N., and Cugny, B., vol. 12777, p. 127771F, International Society for Optics and Photonics, SPIE, https://doi.org/10.1117/12.2689286, 2023.